Available online at www.sciencedirect.com

SciVerse ScienceDirect

Ceramics International 39 (2013) 1775–1783

CERAMICS INTERNATIONAL

www.elsevier.com/locate/ceramint

Investigation of dielectric relaxation behavior of electrospun titanium dioxide nanofibers using temperature dependent impedance spectroscopy

S.S. Batool[a,b,*], Z. Imran[a,b], M.A. Rafiq[a,*], M.M. Hasan[a], M. Willander[b]

[a] *Micro and Nano Devices Group, Department of Metallurgy and Materials Engineering, Pakistan Institute of Engineering and Applied Sciences, PO Nilore, Islamabad 45650, Pakistan*

[b] *Department of Science and Technology, Campus Norrköping, Linköping University, SE-60174 Norrköping, Sweden*

Received 4 July 2012; received in revised form 9 August 2012; accepted 9 August 2012
Available online 29 August 2012

Abstract

The electrospinning method has been utilized in the fabrication of titanium dioxide nanofibers (TNFs) with an average diameter of ~50 nm and length of ~100 μm. Effect of temperature on the dielectric relaxation behavior of the fabricated nanofibers have been studied using AC impedance spectroscopy. The morphological, structural and compositional aspects as well as the optical properties of the TNFs have been investigated by field emission scanning electron microscopy (FESEM), transmission electron microscopy (TEM), energy-dispersive x-ray spectroscopy (EDX) and ultraviolet–visible (UV–vis) absorption spectrum. The permittivity behavior of the device at the frequency below 10^2 Hz shows the relaxation contribution along with the electrode polarization. Dielectric loss peak in loss tangent also confirms the presence of relaxing dipoles in TNFs. The AC conductance as a function of frequency confirms the semiconducting nature of TNFs and obeys Jonscher's power law except a small deviation in the low frequency region. DC conductivity increases with increase in temperature.

Keywords: Titanium dioxide; Electrospinning; Dielectric; DC conductivity

1. Introduction

The synthesis of one-dimensional nanostructures and related research activities has been fueled up with their increasing potential applications and understanding of fundamental concepts [1]. One of the most unique properties of nanomaterials is the mobility of electrons and holes in semiconductors and generally covered by the well-known mechanism of quantum confinement. The transport properties related to phonons and photons have strong correlation with the physical dimensions and the geometry of the material [2,3]. Titanium dioxide (TiO_2) is a semiconducting material and attracted a huge attention due to its wide band gap (~3.00 to 3.5 eV) and high refractive index ($n_{rutile}=2.49$ and $n_{anatase}=2.52$) [4,5]. However, the band gap of the semiconducting materials can be tailored by changing several parameters such as, the phase transition, the density of the impurities, shape, size and surface of the material [6]. The nanodevices of TiO_2 have gained remarkable importance with their increasing applications in the fields of science and technology [7,8].

Titanium dioxide belongs to a class of materials which holds good electrical conductivity as well as dielectric properties with optical transparency. The combination of these properties brings it to the forefront for diverse applications, such as photoelectronic, photocatalytic and, chemical and biosensing applications [9]. In recent years, the investigations about alternating current (AC) electrical characteristics of the organic and inorganic materials compared to the direct current (DC) electrical characteristics are very rare [10].

*Corresponding author at: Micro and Nano Devices Group, Department of Metallurgy and Materials Engineering, Pakistan Institute of Engineering and Applied Sciences, PO Nilore, Islamabad 45650, Pakistan
**Corresponding author.
E-mail addresses: sitwat_naqvi@yahoo.com, fac221@pieas.edu.pk (S.S. Batool).

0272-8842/$ - see front matter © 2012 Elsevier Ltd and Techna Group S.r.l. All rights reserved.
http://dx.doi.org/10.1016/j.ceramint.2012.08.024

Specifically, various TiO_2 nanostructures are being synthesized and hold tremendous interest in the AC electrical properties [11–14]. Additionally, the investigation of dielectric relaxation in electrospun TiO_2 nanofibers has never been reported yet.

Among diverse convoluted techniques, electrospinning is a superficial and a resourceful technique for the fabrication of nanofibers which is highly advantageous for the production of heterojunction through the metal doping and in order to reduce the size of the devices [6,15,16]. Moreover, the process of electrospinning provides handy control to achieve the fabrication of single nanofiber, uniaxial arrays and multilayer of the nanofibers. This controlled fabrication of nanofibers illustrates the fascinating performance due to their high surface area to volume ratio, flexibility in functionalities, enhances the choice of the substrates and superior mechanical properties [17,18].

2. Experimental

Precursor solution for TNFs was prepared by dissolving 0.45 g of Polyvinylpyrrolidone (PVP, M_W = 13,00,000) in 7.5 ml of ethanol and stirred thoroughly for 15 min. Subsequently, the solution was prepared with the mixture of 3 ml acetic acid (CH_3COOH), 3 ml of ethanol (C_2H_6O) and 1.5 ml of titanium tetraisopropoxide ($Ti\{OCH(CH_3)_2\}_4$), and the resulting solution is stirred for 1 h. To avoid the possible reaction between the titanium tetraisopropoxide with the atmospheric moisture, the whole procedure for the preparation of the solution was carried out in the glove box. Electrospinning of TNFs is carried out at ambient condition using a 0.511 mm diameter stainless steel needle with a spinning distance of 7 cm, driven by a voltage of 10 kV. PVP/$Ti\{OCH(CH_3)_2\}_4$ nanofibers are collected on aluminum foil and left in the air for 24 h for the hydrolysis of $Ti\{OCH(CH_3)_2\}_4$. Subsequently, annealing for 3 h at 600 °C in air with heating rate of 10 °C/min is performed to achieve the PVP free TNFs. The dielectric properties of the resulting TNF were measured using broadband dielectric spectrometer at the logarithmic frequency range 10^{-1}–10^{6} Hz in the temperature range of 333–513 K. The preparation of the device was carried out through the dip coating of the TNFs suspended solution in isopropanol. Glass sheet was chosen as a substrate due to its dielectric nature and thermal evaporator was utilized to deposit the aluminum electrodes and separation of 25 μm between the aluminum electrodes was ensured using a patterned mask as shown in Fig. 1. Characterization tools such as field emission scanning electron microscope (FESEM), transmission electron microscope (TEM), ultraviolet–visible (UV–vis) spectroscopy and broad-band dielectric spectrometer were used to investigate the morphological study, crystalline quality, optical band gap and dielectric properties of the TNFs.

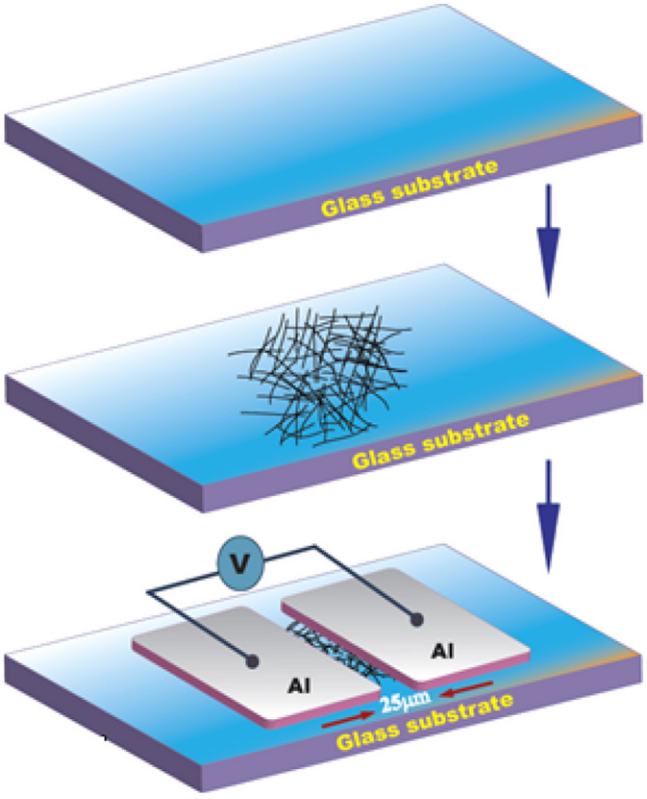

Fig. 1. The schematic images of stepwise fabrication process of the device.

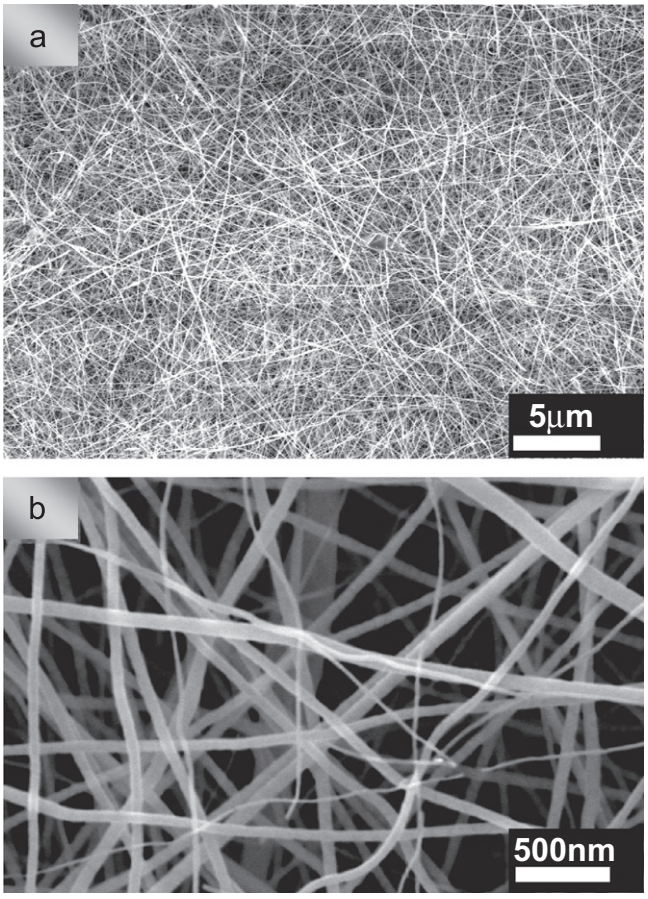

Fig. 2. FESEM images depicting surface morphology and uniform cross-sectional thickness of the TNF nanofibers after calcinations at 600 °C; (a) low magnified image and (b) high magnified image.

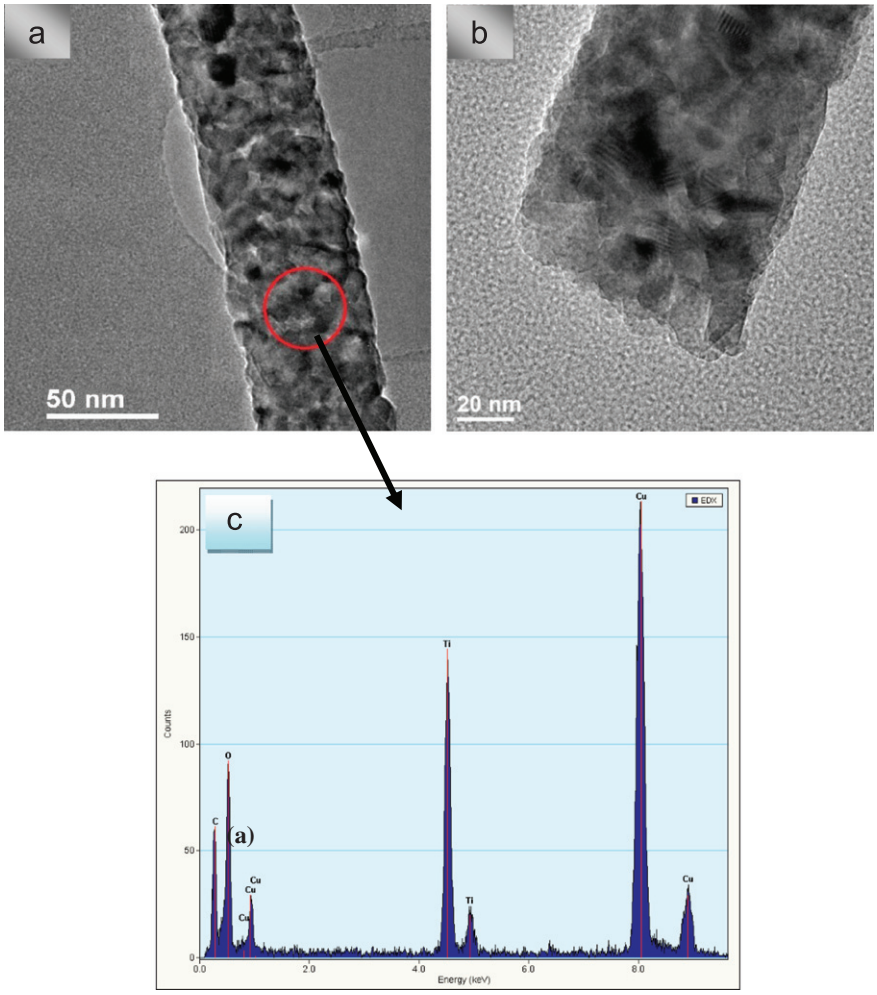

Fig. 3. Bright field micrograph of (a) TNF having a thickness of 50 nm, (b) HRTEM image of TNF calcined at 600 °C and (c) EDX spectrum shows the elemental composition of the selected area of the TNF.

3. Results and discussion

3.1. Scanning electron microscopy

Fig. 2(a) shows the panoramic view of FESEM image which reveals that one-dimensional nanofibers fabricated through the electrospinning method have the length of the several tens of micrometer and an average diameter of 50 nm. However, the high magnification image (Fig. 2(b)) confirms the uniformity and bead free morphology of nanofibers. The bead free morphology can be attributed to the solvent composition of ethanol/acetic acid (15:1) which has reduced surface tension [19].

3.2. Transmission electron microscopy

The TEM image recorded with low resolution (LRTEM) is shown in Fig. 3(a). The obtained results are highly corroborating with the FESEM results and verify the uniformity of the nanofibers have an average diameter of ~50 nm. Black and white spots in the image (Fig. 3(a)) can be related to the presence of the grains with different sizes

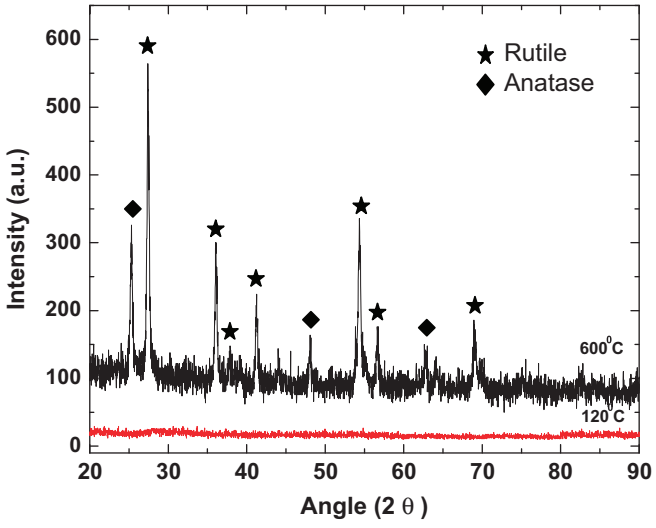

Fig. 4. XRD spectrum of TiO_2 nanofibers annealed at 120 °C for 1 h and 600 °C for 3 h.

and number of defects on the surface walls as well as in the bulk which could lead to the conclusion that the surface of TNFs is rough and porous. The composition of TNFs is

analyzed using EDX from the encircled area of Fig. 3(a) which shows strong peaks related to titanium and oxygen component as seen in Fig. 3(c). Copper and carbon related peaks can be assigned to sample holder (copper grid) and a carbon layer in the sample holder, respectively. The high resolution TEM (HRTEM) image of the TNFs is shown in Fig. 3(b) which indicates that the atomic layers manifest themselves as a series of parallel lines; however, the diverse orientation of these lines. The difference in the growth orientation can be related to the polycrystalline (both rutile and anatase phases) structures of the TNFs.

3.3. X-ray diffraction

The phase evolution and crystal structure of the TNFs are analyzed by x-ray diffraction as shown in Fig. 4. It is obvious from XRD spectra that the TNFs annealed at 600 °C show sharp peaks related to the anatase and rutile phases of the titanium dioxide, however, pre-annealed sample is found as an amorphous in nature.

3.4. UV–vis absorption spectroscopy

Fig. 5 shows the optical absorbance spectrum recorded from TNFs suspension prepared in isopropanol solution for the range of 200–800 nm. Ultraviolet–visible absorption spectrometer has been used to calculate the band gap energy of the TNFs. The absorption spectrum contains two peaks at the positions of 210 nm and 360 nm. The origin of the former peak could be assigned to the presence of the impurities in the TNFs. Extrapolating the second absorption peak gives the estimation of band gap energy i.e. ~3.4 eV which is portrayed in Fig. 5(a). To calculate the absorption peak edge, we traced $(\alpha hv)^2$ as a function of incident photon energy (hv) in Fig. 5(b), as given by the

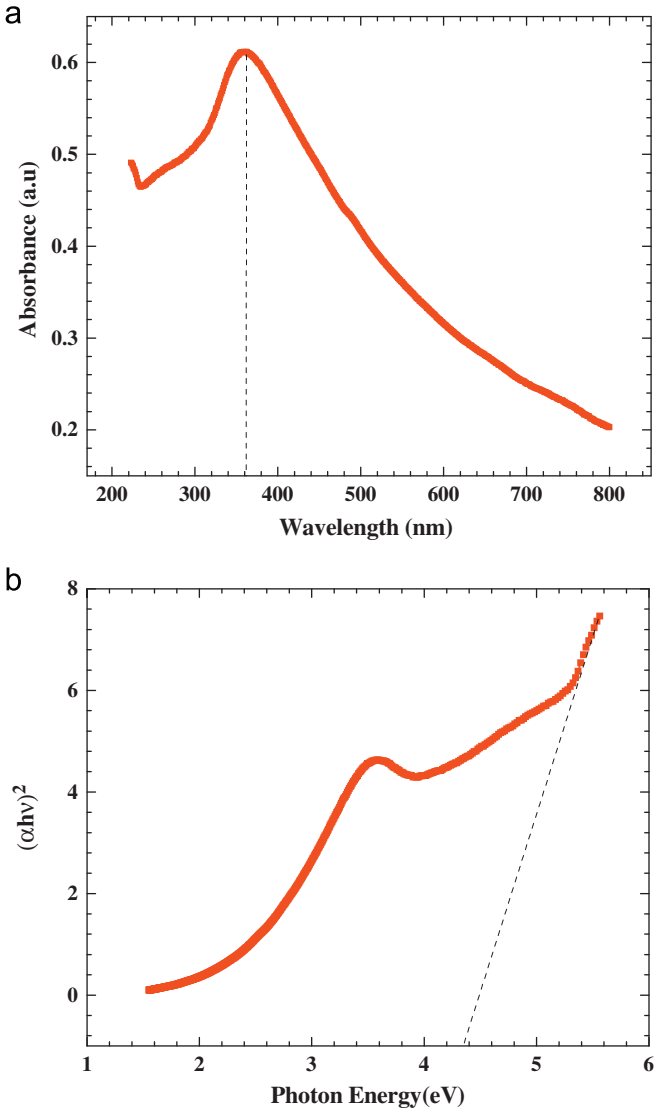

Fig. 5. (a) The UV–vis absorption spectra of TNF at room temperature (b) plot of $(\alpha hv)^2$ as a function of photon energy E_g.

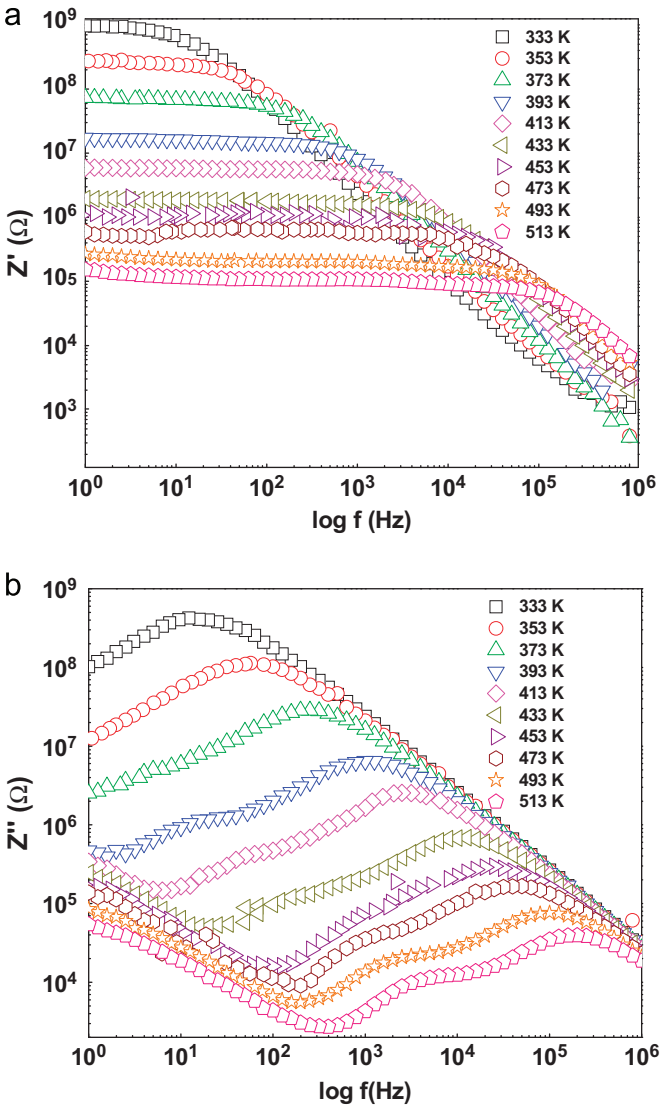

Fig. 6. Z' vs. $\log f$ at different measurement temperatures of TNFs (b) Z'' vs. $\log f$ at different measurement temperatures of TNFs.

relation

$$(\alpha hv)^2 = A(hv - E_g) \quad (1)$$

where 'α' is the absorption coefficient, 'hv' is the photon energy $E_{photon} = 1239/\lambda$, '$A$' is the absorption constant for direct transition and 'E_g' is the band gap energy [20]. The optical band gap energy of 4.12 eV for the TNFs is calculated from the x intercept found by extrapolating the straight portion of the graph in Fig. 5(b). As anticipated from the estimated value of the band gap, the blue shift in the calculated value of the band gap for TNFs compared to the bulk TiO_2 is observed (i.e. approximately 3.2 eV) which could be related to the reduction in the size of the material. This reduction in the size of the material could shift the conduction band in an upward direction and valence band can move in a downward direction; however, the increase in the magnitude of band gap energy has a strong dependence on the effective mass of electrons and holes [21,22]. So, the quantum confinement model can be used to calculate the band gap shift of TNFs compared to bulk material and the size dependent band gap is described as follows:

$$\Delta E_g = \frac{h^2}{2r^2}\left(\frac{1}{|m_e|} + \frac{1}{|m_h|}\right) - \frac{1.8e^2}{\varepsilon_r} \quad (2)$$

$$\Delta E_g = \frac{h^2}{2\mu r^2} - \frac{1.8e^2}{\varepsilon_r} \quad (3)$$

where m_e and m_h are the effective masses of electron and hole respectively, μ is the reduced mass and r is the radius of nanofibers where h represents Plank's constant [23]. For TiO_2 bulk material, the effective mass of electron m_e can vary between 5 m_o and 30 m_o and the mass of the hole is more than 3 m_o, where $m_o = 9.11 \times 10^{-31}$ kg is the free electron rest mass and m_r is the dielectric constant (for TiO_2 bulk = 184) [9,24]. However, the estimated size dependent band gap shift is calculated approximately 0.03 eV for the TNFs while the values of $m_e = 5\ m_o$, $m_h = 3\ m_o$ and $\mu = 1.875\ m_o$.

3.5. Dielectric measurements

To analyze the electrical and dielectric properties of TNFs and their interfaces with electronically conducting electrodes at different temperatures (333–513 K) in the frequency range from 1 Hz–1 MHz, the complex impedance method has been used. The variation of real (Z') and imaginary (Z'') parts of the impedance with frequency Fig. 6(a and b) and Z' vs. Z'' impedance is depicted in Fig. 7. Fig. 6(a) shows the variation of Z' with frequency at different temperatures (333–513 K), which indicates that

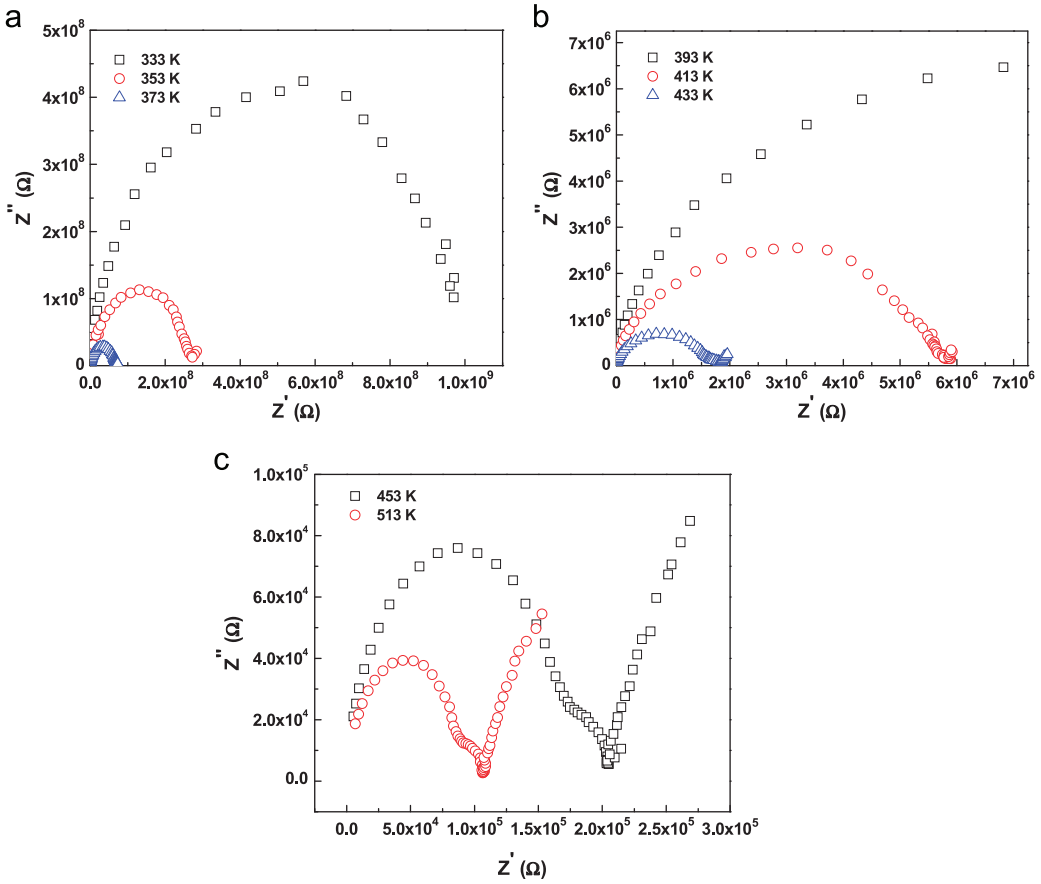

Fig. 7. Z' vs. Z'' at different measurement temperatures of TNFs (a) 333–373 K, (b) 393–433 K, and (c) 453–513 K.

both frequency and temperature cause a decrease in electrical resistance as Z' correspond to electrical resistance. Temperature independent behavior on Z' at higher frequencies suggesting the possible release of space charge and a consequence of lowering of potential barrier [25,26]. To evaluate the suitable relaxation frequency we present the variation of Z'' with frequency at different temperatures in Fig. 6(b). It is observed that two peaks appear above the temperature 413 K, representing the presence of at least two dielectric relaxation processes at those temperature values. The positions of peak shift towards higher frequencies with increase of temperature and the absolute value of Z'' decreases with temperature. At higher temperatures there could be a possibility of third relaxation peak at very low frequency. To examine the detailed relaxation phenomena in TNFs, the impedance spectra at three different temperatures ranges from 333 to 373 K, 393 to 433 K and 453 to 513 K are shown in Fig. 7(a), (b) and (c) respectively. These are characterized by the appearance of a semicircular arc at different temperatures followed by a spur at lower frequencies at all temperatures. Moreover, two semicircles are observed for TNFs at higher temperatures (Fig. 7(c)), indicating the presence of aforementioned two relaxation behaviors (Fig. 6) [27]. The impedance spectra having spur in the low frequency region are due to the surface related artifacts between electrode and sample and may also represent electrode polarization effect [28]. As temperature increases, the radius of the arc corresponding to the bulk resistance of the sample decreases indicating a thermally activated conduction mechanism.

Fig. 8 (a,b) illustrates the variation of dielectric constant (ε') and dielectric loss ($\tan\delta$) for the TNFs at various temperatures as a function of frequency, respectively. ε' at lower frequencies is rather high and is found to decrease with frequency and at higher frequencies it becomes almost stabilized; it is also increased by raising the measuring temperature (Fig. 8 (a)). The variation in the nature of ε' in the presence of an alternating electric field may be described in the following way. Oscillation of free dipoles in AC field causes a change in ε', at very low frequencies these dipoles follow the field and we get ε' at quasi-static fields. With the increase in frequency, the electric field begins to lead by the dipoles which may cause a slight decrease in ε' but at higher frequencies, these dipoles cannot follow the field and we get frequency independent ε' [29]. The high dispersion of ε' at low frequency at all temperatures may also be attributed to the formation of the space charge region at the electrode interface which is commonly known as non-Debye nature of behavior [30]. Fig. 8(b) shows a plot between $\log f$ and $\tan\delta$, in which a relaxation peak appears in the low frequency region which shifts towards higher frequencies along with a slight increase in height by increasing temperature. Increasing temperature has the effect of mobilizing the free charges, reducing pinning and leading to greater amount of charges participating relaxation process at a fixed frequency [31]. Usually, in the lower conductivity system electrode polarization can

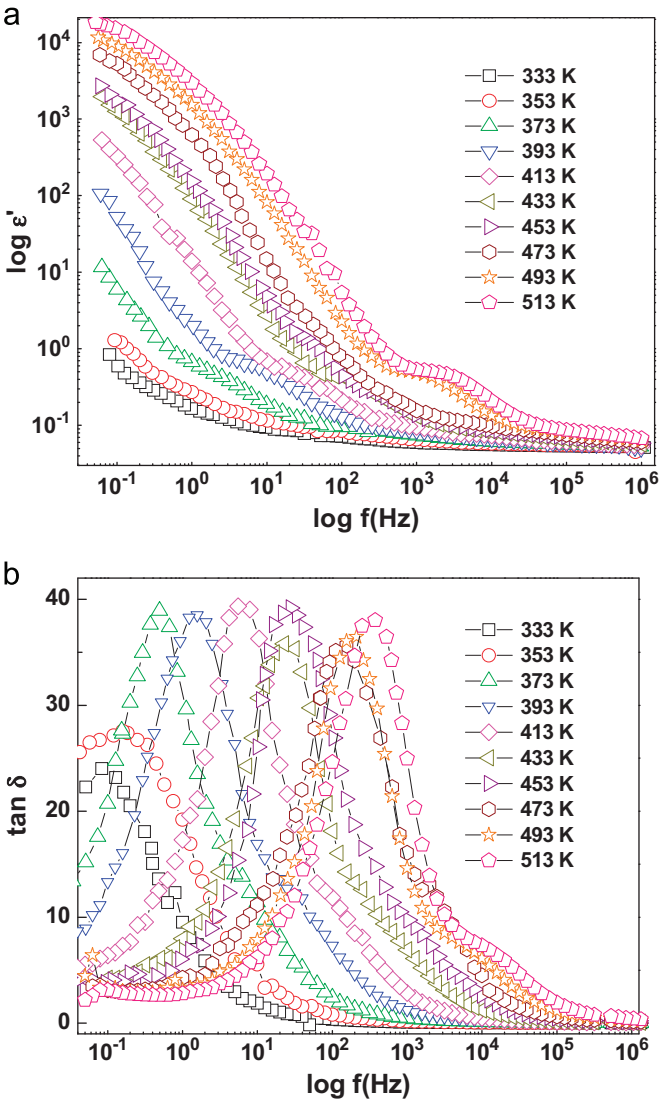

Fig. 8. Variation of (a) dielectric constant (M') and (b) dielectric loss ($\tan\delta$) for TNFs at various temperatures as a function of frequency.

completely mask the low frequency relaxation [32]. In order to study the dielectric relaxations and to resolve the low frequency relaxation, electric modulus formalism is used.

The complex electric modulus spectrum (M' vs. M'') have been carried out in selected temperature range 333–513 K is shown in Fig. 9(a). Complex electric modulus can help in analyzing the electrical response of TNFs through polarization analysis. One semicircle can be observed in Fig. 9(a) for all the temperatures with a smaller shift towards higher M'' values. This behavior could be related to the decrease in modulus resistance with the increase of temperature in good agreement with the literature [33]. Variation of real (M') and imaginary (M'') parts of the electric modulus as a function of frequency of various temperatures have been depicted in Fig. 9(b) and (c), respectively. M'' shows a constant value at higher frequencies while at lower frequencies it approaches to zero for all temperatures. But shows dispersion in the intermediate

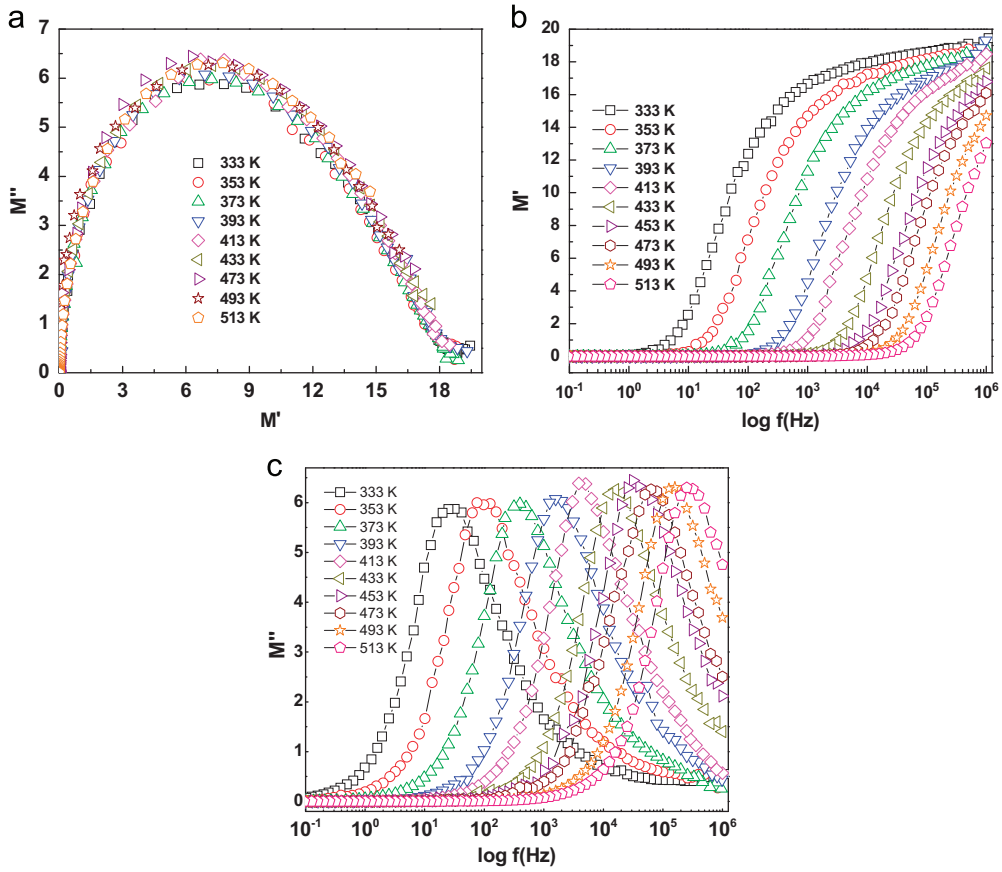

Fig. 9. (a) Cole–Cole plots between M' and M'' for TNFs at different temperatures; (b) variation of real part of M' with frequency at different temperatures; and (c) variation of imaginary part of M'' with frequency at different temperatures.

frequencies which increases as temperature increases. While M'' exhibits a single broad relaxation peak centered in the dispersion region of M' in the temperature range studied. The broad nature of the peak is consequence of distribution of relaxation time which shifts towards higher frequencies as temperature increases, confirms the relaxation phenomenon is thermally activated and the frequency region under the curve determines the region in which charge carriers are mobile on long distances [32]. The region where the peak occurs indicating the transition from the long range to short range mobility with increase in frequency as the region below the peak maximum determine the range in which carriers are mobile over long distance and above the peak they are confined to potential barriers, being mobile over short distances [34]. This type of behavior suggests the existence of a temperature dependent hoping type mechanism of charge transport. The effect of temperature on relaxation process is further analyzed by plotting the maximum peak frequency in the imaginary part of modulus spectra against the reciprocal of temperature. Fig. 10 shows the activation energy plot of TNFs for the relaxation process observed. It is analyzed from the plot (inset of Fig. 10) that increases in temperature causes decrease in relaxation time due to enhancement of mobility of charge carriers at high temperature. It can

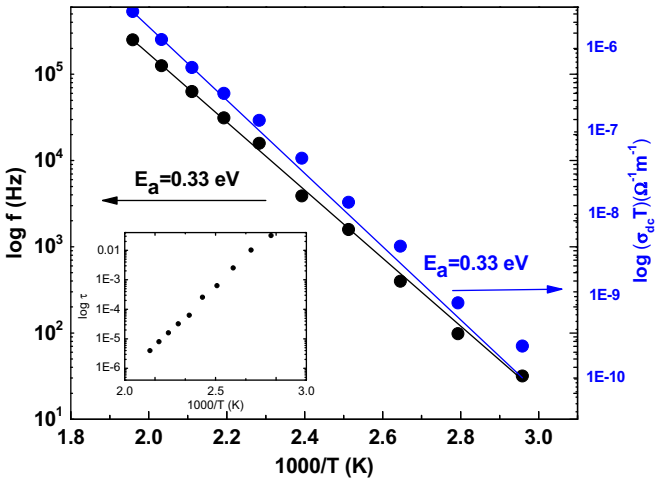

Fig. 10. Arrhenius plot shows the dependence of the σ and f_{max} (peak) vs. 1000 T^{-1} of TNFs.

be further well described by the Arrhenius type behavior. Arrhenius equation is used to calculate the activation energy from the slope of the dielectric relaxation line plot in Fig. 10:

$$f = f_o \exp\left(-\frac{E_a}{kT}\right) \quad (4)$$

where f is the frequency maximum in the imaginary part of modulus spectrum, E_a is the activation energy and k is the Boltzmann constant. The activation energy was calculated for dielectric relaxation TNFs is 0.33 eV.

The paramount changes in the features of AC conductivity (o'_{ac}) as a function of logarithmic frequency at different temperatures could be seen in Fig. 11, which shows the conductivity increases with rising temperature. In the low frequency region, the behavior of conductivity is frequency independent and it becomes sensitive at high frequency region. This behavior can be roughly described by a power law by the expression which can be used to fit a solid line in the AC conductivity with respect to frequency [35]:

$$\sigma = O'_o + A\omega^n \tag{5}$$

where 'o'_o' is the DC conductivity (o'_{dc}) (which is independent of frequency extracted from the low frequency plateau), 'ω' is the angular frequency, 'A' is the pre-exponential factor and 'n' is the fractional exponent respectively. Effect of temperature on these parameters is given in Table 1, which shows a decrease in value of 'n' with temperature. It is reported [36] that when the value of 'n' is greater than 1, it means the motion involved localized hopping without the

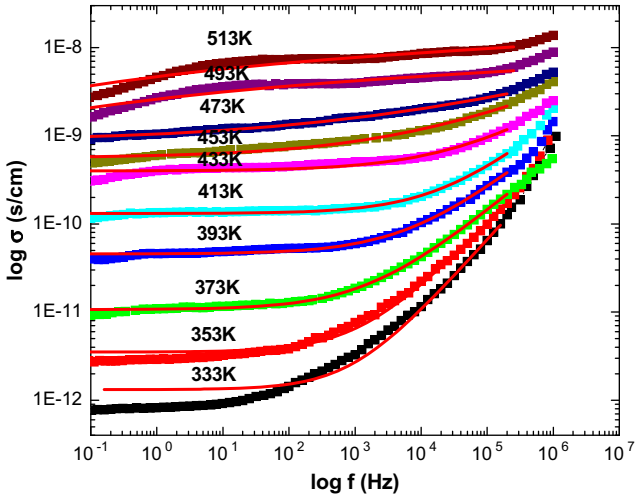

Fig. 11. Frequency dependence of the AC conductivity of TNFs at various temperatures.

Table 1.
Data of DC conductivity, A and n at different temperatures.

Temperature (K)	o'_o	A	n
333	1.31995E−12	4.26620E−15	0.83678
353	3.52337E−12	1.55721E−14	0.76072
373	1.06859E−11	1.04213E−13	0.62233
393	4.56989E−11	2.22571E−13	0.60031
413	1.31350E−10	2.70661E−13	0.57142
433	3.19919E−10	2.58651E−12	0.46768
453	5.64793E−10	3.40133E−11	0.31563
473	8.68763E−10	1.80199E−10	0.20234
493	2.61633E−06	1.11321E−09	0.00009
513	5.50824E−05	1.70125E−06	0.00004

spices leaving the neighborhood and when 'n' is less than 1, diffusion limited hopping involves. Therefore, the transport mechanism is explained by the thermally activated hopping process between two sites separated by an energy barrier. Using the Arrhenius relation, $o'_{dc}T = o'_o \exp[-E_a/kT]$ where, o'_o is the pre-exponential factor, E_a is the activation energy related to this conduction process, k is the Boltzmann constant and T is the temperature, gives the activation energy at 0.33 eV (Fig. 10).

4. Conclusions

Semiconducting TNFs with an average diameter and length of ~50 nm and ~100 μm, respectively, have been fabricated using a facile and reproducible electrospinning technique. The higher band gap energy (~4.2 eV) compared to the bulk material could be the result of a quantum size effect. The temperature and frequency dependence of dielectric properties shows that the AC conductivity and relaxation are dominated by hopping of charge carriers and dipoles respectively. Complex impedance analysis in the temperature range 333–513 K and frequency range 10^{-1}–10^{6} Hz indicates the non-Debye relaxation type of relaxation process and the presence of relaxation time distribution as well as the electrode polarization effects.

Acknowledgments

We acknowledge the financial support of the Higher Education Commission (HEC), Pakistan.

References

[1] V. Thavasi, G. Singh, S. Ramakrishna, Electrospun nanofibers in energy and environmental applications, Energy and Environmental Science 1 (2008) 205–221.
[2] C.B. Murray, C.R. Kagan, M.G. Bawendi, Synthesis and characterization of monodisperse nanocrystals and close-packed nanocrystal assemblies, Annual Review of Materials Science 30 (2000) 545–610.
[3] Y. Yin, A.P. Alivisatos, Colloidal nanocrystal synthesis and the organic–inorganic interface, Nature 437 (2005) 664–670.
[4] W.D. Kingrey, H.K. Bowen, D.R. Uhlmann, in: Introduction to Ceramics, 2nd ed., John Wiley, New York, 1976.
[5] K. Das, S.N. Sharma, M. Kumar, S.K. De, Morphology dependent luminescence properties of Co doped TiO_2 nanostructures, Journal of Physical Chemistry C 113 (2009) 14783–14792.
[6] S. Ramakrishna, A. Kumar, R. Jose, K. Fujihara, J. Wang, Structural and optical properties of electrospun TiO_2 nanofibers, Chemistry of Materials 19 (2007) 6536–6542.
[7] T. Kasuga, M. Hiramatsu, A. Hoson, T. Sekino, K. Niihara, Formation of titanium oxide nanotube, Langmuir 14 (1998) 3160–3163.
[8] I. Robel, V. Subramanian, M. Kuno, P.V. Kamat, Quantum dot solar cells harvesting light energy with CdSe nanocrystals molecularly linked to mesoscopic TiO_2 films, Journal of the American Chemical Society 128 (2006) 2385–2393.
[9] X. Chen, S.S. Mao, Titanium dioxide nanomaterials: synthesis, properties, modifications, and applications, Chemical Reviews 107 (2007) 2891–2959.
[10] F. Yakuphanoglu, Y. Aydogdu, U. Schatzschneider, E. Rentschler, DC and AC conductivity and dielectric properties of the metal-radical

compound: aqua[bis(2-dimethylaminomethyl-4-NIT-phenolato)]copper(II), Solid State Communications 128 (2003) 63–67.
[11] A.W. Xu, Y. Gao, H.Q. Liu, The preparation, characterization, and their photocatalytic activities of rare-earth-doped TiO_2 nanoparticles, Journal of Catalysis 207 (2002) 151–157.
[12] G.K. Mor, O.K. Varghese, M. Paulose, N. Mukherjee, C.A. Grimes, Fabrication of tapered, conical-shaped titania nanotubes, Journal of Materials Research 18 (2003) 2588–2593.
[13] Y. Lin, G.S. Wu, X.Y. Yuan, T. Xie, L.D. Zhang, Fabrication and optical properties of TiO_2 nanowire arrays made by sol–gel electrophoresis deposition into anodic alumina membranes, Journal of Physics: Condensed Matter 15 (2003) 2917–2922.
[14] D. Li, Y.N. Xia, Fabrication of titania nanofibers by electrospinning, Nano Letters 3 (2003) 555–560.
[15] S. Barth, F. Hernandez-Ramirez, J.D. Holmes, A. Romano-Rodriguez, Synthesis and applications of one-dimensional semiconductors, Progress in Materials Science 55 (2010) 563–627.
[16] Heping Li, Wei Zhang, W. Pan, Enhanced photocatalytic activity of electrospun TiO_2 nanofibers with optimal anatase/rutile ratio, Journal of the American Ceramic Society 94 (2011) 3184–3187.
[17] J.J. Mack, L.M. Viculis, A. Ali, R. Luoh, G.L. Yang, H.T. Hahn, F.K. Ko, R.B. Kaner, Graphite nanoplatelet reinforcement of electrospun polyacrylonitrile nanofibers, Advanced Materials 17 (2005) 77–80.
[18] R. Siddheswaran, R. Sankar, M.R. Babu, M. Rathnakumari, R. Jayavel, P. Murugakoothan, P. Sureshkumar, Preparation and characterization of ZnO nanofibers by electrospinning, Crystal Research and Technology 41 (2006) 446–449.
[19] Z.M. Huang, Y.Z. Zhang, M. Kotaki, S. Ramakrishna, A review on polymer nanofibers by electrospinning and their applications in nanocomposites, Composites Science and Technology 63 (2003) 2223–2253.
[20] P.K. Ghosh, U.N. Maiti, K.K. Chattopadhyay, Structural and optical characterization of US nanofibers synthesized by dc-sputtering technique, Materials Letters 60 (2006) 2881–2885.
[21] H. Higashiyama, F. Tokunaga, Cause of the blue shift of the absorption-spectrum of tetranitromethane-treated bacteriorhodopsin, FEBS Letters 218 (1987) 287–291.
[22] D.J. Mowbray, R.A. Hogg, M.S. Skolnick, M.C. Delong, S.R. Kurtz, J.M. Olson, Valence-band splitting in ordered $Ga_{0.5}In_{0.5}P$ measured by polarized photoluminescence excitation spectroscopy, Physical Review B 46 (1992) 7232–7235.
[23] H.S. Lee, C.S. Woo, B.K. Youn, S.Y. Kim, S.T. Oh, Y.E. Sung, H.I. Lee, Bandgap modulation of TiO_2 and its effect on the activity in photocatalytic oxidation of 2-isopropyl-6-methyl-4-pyrimidinol, Topics in Catalysis 35 (2005) 255–260.
[24] N. Serpone, D. Lawless, R. Khairutdinov, Size effects on the photophysical properties of colloidal anatase TiO_2 particles—size quantization or direct transitions in this indirect semiconductor, Journal of Physical Chemistry 99 (1995) 16646–16654.
[25] A. Kumar, B.P. Singh, R.N.P. Choudhary, A.K. Thakur, Characterization of electrical properties of Pb-modified $BaSnO_3$ using impedance spectroscopy, Materials Chemistry and Physics 99 (2006) 150–159.
[26] B. Behera, P. Nayak, R.N.P. Choudhary, Impedance spectroscopy study of $NaBa_2V_5O_{15}$ ceramic, Journal of Alloys and Compounds 436 (2007) 226–232.
[27] J.-H. Hwang, K.S. Kirkpatrick, T.O. Mason, E.J. Garboczi, Experimental limitations in impedance spectroscopy: Part IV. Electrode contact affects, Solid State Ionics 98 (1997) 93–104.
[28] S. Vinoth Rathan, G. Govindaraj, Thermal and electrical relaxation studies in $Li_{(4+x)}Ti_xNb_{1-X}P_3O_{12}$ ($0.0 \leq X \leq 1.0$) phosphate glasses, Solid State Sciences 12 (2010) 730–735.
[29] S. Vinoth Rathan, G. Govindaraj, Electrical relaxation studies on $Na_2NbMP_3O_{12}$ (M=Zn, Cd, Pb and Cu) phosphate glasses, Materials Chemistry and Physics 120 (2010) 255–262.
[30] T. Badapanda, V. Senthil, S.K. Rout, L.S. Cavalcante, A.Z. SimÃµes, T.P. Sinha, S. Panigrahi, M.M. de Jesus, E. Longo, J.A. Varela, Rietveld refinement, microstructure, conductivity and impedance properties of $Ba[Zr_{0.25}Ti_{0.75}]O_3$ ceramic, Current Applied Physics 11 (2011) 1282–1293.
[31] D. Arun Kumar, S. Selvasekarapandian, H. Nithya, A. Sakunthala, M. Hema, Dielectric, modulus and impedance analysis of LaF_3 nanoparticles, Physica B: Condensed Matter 405 (2010) 3803–3807.
[32] C.V. Chanmal, J.P. Jog, Dielectric relaxations in PVDF/$BaTiO_3$ nanocomposites, Express Polymer Letters 2 (2008) 294–301.
[33] X. Wang, J. Zhuang, Q. Peng, Y. Li, A general strategy for nanocrystal synthesis, Nature 437 (2005) 121–124.
[34] M.M. Costa, J.G.F.M. Pires, A.J. Terezo, M.P.F. Graca, A.S.B. Sombra, Impedance and modulus studies of magnetic ceramic oxide $Ba_2Co_2Fe_{12}O_{22}$ (Co_2Y) doped with Bi_2O_3, Journal of Applied Physics 110 (2011) 034107.
[35] D.K. Pradhan, R.N.P. Choudhary, B.K. Samantaray, Studies of dielectric relaxation and AC conductivity behavior of plasticized polymer nanocomposite electrolytes, International Journal of Electrochemical Science 3 (2008) 597–608.
[36] G. Desgardin, C. Robert, D. Groult, B. Raveau, Une nouvelle famille structurale: les titanoniobates titanotantalates $A_2Nb_6TiO_{18}$ et $A_2Ta_6TiO_{18}$, Journal of Solid State Chemistry 22 (1977) 101–111.